

Hierarchical Neural Semantic Representation for 3D Semantic Correspondence

KEYU DU*, University of Electronic Science and Technology of China, China

JINGYU HU*†, The Chinese University of Hong Kong, HK SAR, China

HAIPENG LI, University of Electronic Science and Technology of China, China

HAO XU, The Chinese University of Hong Kong, HK SAR, China

HAIBIN HUANG, TeleAI, China

CHI-WING FU, The Chinese University of Hong Kong, HK SAR, China

SHUAICHENG LIU, University of Electronic Science and Technology of China, China

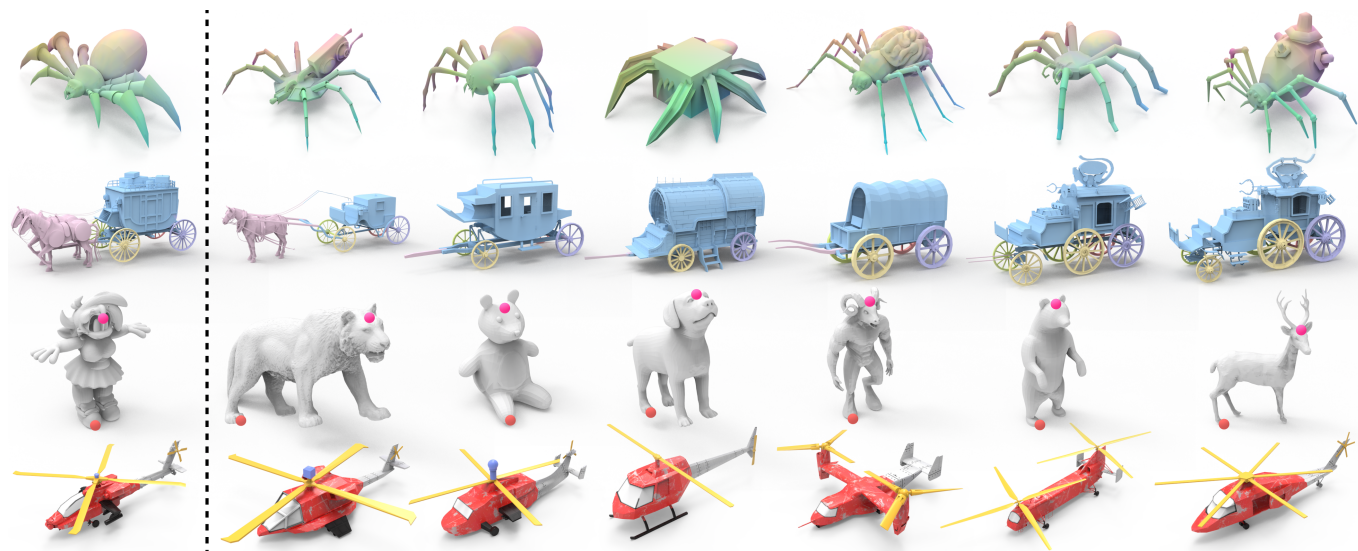


Fig. 1. Our new framework is capable of predicting robust 3D correspondence between shapes of varying topological structures and geometric complexities, such as variations in the spider body and leg numbers (top row), the presence/absence of horses (2nd row), and variations in the main rotors of the helicopters (last row). Our framework also supports various applications: shape co-segmentation (2nd row), keypoint matching (3rd row), and texture transfer (last row).

This paper presents a new approach to estimate accurate and robust 3D semantic correspondence with the hierarchical neural semantic representation. Our work has three key contributions. First, we design the hierarchical neural semantic representation (HNSR), which consists of a global semantic feature to capture high-level structure and multi-resolution local geometric features to preserve fine details, by carefully harnessing 3D priors from pre-trained 3D generative models. Second, we design a progressive global-to-local matching strategy, which establishes coarse semantic correspondence using the global semantic feature, then iteratively refines it with local geometric features, yielding accurate and semantically-consistent mappings. Third, our framework is training-free and broadly compatible with various pre-trained 3D generative backbones, demonstrating strong generalization

across diverse shape categories. Our method also supports various applications, such as shape co-segmentation, keypoint matching, and texture transfer, and generalizes well to structurally diverse shapes, with promising results even in cross-category scenarios. Both qualitative and quantitative evaluations show that our method outperforms previous state-of-the-art techniques.

CCS Concepts: • Computing methodologies → Shape analysis; Neural networks.

Additional Key Words and Phrases: 3D semantic correspondence, shape representation

1 INTRODUCTION

Establishing semantic correspondence between 3D shapes [Van Kaick et al. 2011] has broad application values in computer graphics, *e.g.*, shape analysis [Sidi et al. 2011], texture transfer [Dinh et al. 2005], and shape editing [Sumner and Popović 2004; Zhu et al. 2017]. However, accurate semantic-aware 3D correspondences are very challenging to achieve, as we need to build precise mappings between

*Both authors contributed equally to the paper.

†Corresponding author.

Authors' Contact Information: Keyu Du, University of Electronic Science and Technology of China, China; Jingyu Hu, The Chinese University of Hong Kong, HK SAR, China; Haipeng Li, University of Electronic Science and Technology of China, China; Hao Xu, The Chinese University of Hong Kong, HK SAR, China; Haibin Huang, TeleAI, China; Chi-Wing Fu, The Chinese University of Hong Kong, HK SAR, China; Shuaicheng Liu, University of Electronic Science and Technology of China, China.

3D shapes, while attentively considering the topological difference, object categories, and parts semantics, as well as the geometric details. The task becomes even more challenging when handling shapes with missing parts and cross-category differences.

Traditional methods [Huang et al. 2014; Ovsjanikov et al. 2012] typically rely on hand-crafted shape descriptors to match shapes. Hence, they often fall short of generalizing to handle diverse shapes. Later, [Litany et al. 2017a; Marin et al. 2020] propose to learn shape descriptors by using a neural network to detect shape correspondence. However, these methods rely on annotated data, which is labor-intensive to create, and are often limited to specific domains, such as human bodies [Melzi et al. 2019] and animals [Dyke et al. 2020]. Such a narrow focus restricts their capabilities to handle a wider range of shapes with varying topologies and geometry, and thus their applicability in real scenarios.

Very recently, various 3D generative models [Hui et al. 2024; Li et al. 2025; Zhang et al. 2024; Zhao et al. 2025] demonstrate rich semantic and geometric priors learned by pre-trained models when leveraging large-scale 3D shape data [Deitke et al. 2023a,b]. Though these models are designed mainly for shape generation, their latent representations implicitly capture rich geometric and semantic information. Hence, they have great potential values for downstream shape analysis, e.g., 3D semantic correspondence and shape co-segmentation. However, how to effectively exploit 3D generative models for shape analysis remains underexplored.

In this work, we propose a new framework that harnesses pre-trained 3D generative models to construct a **Hierarchical Neural Semantic Representation (HNSR)** for 3D semantic correspondence. Our representation consists of a global semantic feature that captures high-level structural information and a set of local geometric features at multiple resolutions that preserve fine-grained details. These multi-scale features are extracted from a pre-trained 3D generative model. Building on it, we propose a progressive global-to-local matching strategy that first establishes coarse correspondences using a global semantic feature, then refines them with local geometric features. This design effectively enables accurate and robust semantic correspondence between 3D shapes with structural and geometric variations. As the second row of Figure 1 shows, our method achieves consistent shape co-segmentation results, even for shapes with complex topologies and fine geometries. The first and fourth rows present semantic correspondence and texture transfer results, manifesting that our method remains effective, despite missing parts between source and target shapes, demonstrating its strong robustness to structural inconsistency.

Our framework is compatible with a variety of pre-trained 3D generative models, including category-specific diffusion models [Shim et al. 2023; Zheng et al. 2023] and a 3D foundation model [Xiang et al. 2025] trained on large-scale datasets [Deitke et al. 2023a,b]. By exploiting the geometric and semantic priors learned by these models, our method achieves robust performance in diverse settings. Notably, when combined with the 3D foundation model [Xiang et al. 2025], our method exhibits strong generalization to challenging cross-category scenarios. As the third row of Figure 1 shows, our method is able to accurately match semantically corresponding positions such as the human foot and the lion’s paw. In particular, this is achieved in a training-free manner, as our method directly

utilizes features extracted from the 3D generative backbones, *without* requiring additional supervision or task-specific fine-tuning. Both quantitative and qualitative comparisons between our framework and various baselines show its superior performance. Furthermore, we showcase that our framework can be applied in various downstream applications such as shape co-segmentation, keypoint matching, and texture transfer, highlighting its generalizability in real-world 3D shape analysis scenarios.

In summary, our contributions are summarized as follows.

- We introduce a novel **Hierarchical Neural Semantic Representation (HNSR)** by extracting hierarchical features from pre-trained 3D generative models, enabling rich encoding of shape semantics and geometry.
- We propose a progressive global-to-local correspondence matching strategy that starts with coarse semantic matching and progressively refines it for precise correspondence.
- Our method requires no additional training and is compatible with various 3D generative backbones. We demonstrate the effectiveness of our approach through quantitative and qualitative experiments, achieving superior performance over state-of-the-art methods, while also supporting various downstream applications such as shape co-segmentation, keypoint matching, and texture transfer.

2 RELATED WORK

2.1 3D Shape Correspondence

3D shape correspondence [Bronstein et al. 2008; Huang et al. 2008; Kim et al. 2011; Van Kaick et al. 2011] is a fundamental task in computer graphics, aiming at establishing correspondences between 3D shapes. Among the existing works, the functional map emerges as a dominant approach. This approach computes shape descriptors to derive functional maps, which encode shape correspondences as compact representations within the eigenbasis of the Laplace-Beltrami operator (LBO). The traditional pipeline of functional-map-based methods [Eisenberger et al. 2020; Huang et al. 2014; Kovnatsky et al. 2015; Litany et al. 2017b; Nogneng and Ovsjanikov 2017; Ovsjanikov et al. 2012; Ren et al. 2019, 2018; Rodola et al. 2014] typically involves extracting handcrafted descriptors, followed by a functional-map estimation based on the descriptors.

With the advent of deep learning, [Cao and Bernard 2023; Donati et al. 2020; Halimi et al. 2019; Litany et al. 2017a; Roufosse et al. 2019; Sharma and Ovsjanikov 2020; Zhuravlev et al. 2025] utilize the neural network to learn the shape descriptors from shape data in an end-to-end manner. However, a key limitation persists: the reliance on spectral embeddings makes the correspondence quality highly dependent on the stability of the LBO eigenbasis. When the input shapes exhibit significant geometric or topological variations, the spectral decompositions can easily diverge, leading to misaligned eigenbases. This spectral instability propagates errors into the functional map, thereby degrading the correspondence accuracy.

Another line of works [Deng et al. 2021; Eisenberger et al. 2019; Groueix et al. 2018; Sumner and Popović 2004; Zhang et al. 2008; Zheng et al. 2021; Zhu et al. 2017] adopts a deformation-based paradigm, by deforming pre-defined templates to match the target geometry. While anchoring shapes to a common reference leads to a

more consistent shape correspondence, relying on a fixed template limits the approach’s flexibility, making it hard to handle shapes with large topological variations or fine-grained geometric details. To overcome the limitations of existing approaches, we propose the first framework that harnesses the power of pre-trained 3D generative models to establish high-quality 3D semantic correspondence, enabling us to handle shapes with diverse topologies, fine-grained geometric details, and even cross-category variations. In particular, our approach operates in a training-free manner. It generalizes well for different shape classes, even without labeled correspondence data and fine-tuning; see Section 4.5.

2.2 Semantic Correspondence

Semantic correspondence is a relatively new topic, focusing on establishing a meaningful mapping between different instances by locating and matching semantically similar positions. Unlike traditional correspondence methods [Bay et al. 2006; Lowe 2004], which focus on local appearance or geometric similarity, semantic correspondence targets higher-level understanding, aiming at a more robust matching even with variations in geometries, structures, and object categories. Recent works study semantic correspondence mainly on images, e.g., [Jiang et al. 2021; Jin et al. 2021; Lee et al. 2021; Rocco et al. 2018]. Though these methods demonstrate promising results on moderate appearance and pose variations, their performance depends heavily on costly annotated datasets, thus limiting their applicability. More recent methods [Luo et al. 2023; Min et al. 2020; Peebles et al. 2022; Tang et al. 2023; Zhang et al. 2023, 2021] explore unsupervised techniques by making use of pre-trained image generative models [Goodfellow et al. 2014; Ho et al. 2020]. These approaches often utilize spatially-aligned representations and identify semantically-consistent regions based on feature similarity to enable correspondence estimation. Research on 3D semantic correspondence is largely unexplored, with only a few existing works. [Abdelreheem et al. 2023a] propose a two-stage approach that first segments 3D shapes then establishes a mapping between segments to yield a coarse-level semantic correspondence. Yet, the method relies heavily on the quality of the segmentation, so the resulting semantic correspondence is often coarse and imprecise. [Dutt et al. 2024; Liu et al. 2025; Sun et al. 2024; Zhu et al. 2024] establish 3D semantic correspondences by projecting 2D features onto 3D shapes and aggregating the features across views, whereas [Liu et al. 2025; Sun et al. 2024] employ shape registration to construct correspondences. However, as image features lack explicit 3D geometric information, directly transferring them to 3D often leads to noisy and inconsistent predictions.

The above limitations underscore the need for dedicated 3D descriptors that capture both fine-grained geometry and high-level semantics for accurate 3D semantic correspondence. In this work, we design a new approach that operates directly in 3D. We build our representation and perform the correspondence matching *entirely in the 3D space*, bypassing the need to pre-segment the shapes.

2.3 3D Generative Modeling

Recent advances in large-scale 3D datasets such as Objaverse [Deitke et al. 2023b] and Objaverse-XL [Deitke et al. 2023a] have paved the way for the development of 3D foundation models [Hong et al. 2024;

Hui et al. 2024; Li et al. 2025; Xiang et al. 2025; Zhang et al. 2024; Zhao et al. 2025]. These models are capable of generating high-quality and detailed 3D shapes, while generalizing effectively to unseen shapes of complex topologies and intricate details. Such strong generalizability demonstrates the robust shape priors acquired by the models during training. Yet, little has been done on how to effectively harness these powerful geometric priors for downstream shape analysis tasks such as shape co-segmentation and correspondence.

3 METHOD

3.1 OVERVIEW

Given a pair of source \mathcal{S}^{src} and target \mathcal{S}^{tar} shapes, our goal is to establish the 3D semantic correspondence between them. As a prerequisite, both shapes are represented in a voxelized form, which serves as the input to our framework. Figure 2 provides an overview of our two-stage framework:

- **Hierarchical Neural Semantic Representation.** First, we design the hierarchical neural semantic representation (HNSR), denoted as \mathcal{F} , to encode both semantic and geometric information of a 3D shape in a multi-resolution manner. Given input shape \mathcal{S} in voxel form, we extract \mathcal{F} from a pre-trained 3D generative model \mathcal{G} . Specifically, we perturb \mathcal{S} and pass it through \mathcal{G} to extract intermediate features from selected network layers. We then organize these features into global semantic feature \mathcal{F}_G and a set of local geometric features \mathcal{F}_L , forming the HNSR: $\mathcal{F} = (\mathcal{F}_G, \mathcal{F}_L)$.
- **Progressive Correspondence Matching.** Second, we design a progressive global-to-local matching strategy to establish accurate semantic correspondences between 3D shapes. Given the extracted HNSR of the source and target shapes, our method proceeds in two stages: (i) Global Initialization, which computes coarse semantic correspondences using the low-resolution global feature to localize semantically similar regions; and (ii) Local Refinement, which iteratively refines the correspondences using multi-scale local geometric features, progressively narrowing down the matching region at each level. This strategy encourages semantically meaningful and spatially precise correspondences.

3.2 Hierarchical Neural Semantic Representation

Given an input 3D shape \mathcal{S} in a voxel-based representation, our goal is to build the **Hierarchical Neural Semantic Representation (HNSR)** \mathcal{F} , composed of a global semantic feature and a set of local geometric features at multiple resolutions. These multi-scale features are hierarchically extracted from a pre-trained 3D generative model \mathcal{G} and are designed to capture both high-level semantic structures and fine-grained geometric details. We construct the HNSR \mathcal{F} in two stages: (i) *Feature Extraction* and (ii) *HNSR Construction*, as Figure 2(a) illustrates. The specific voxel format of \mathcal{S} (e.g., SDF, occupancy, or latent code) depends on the backbone of the generative model \mathcal{G} . The details of both the input format and the corresponding generative backbones will be provided in Section 3.4.

Feature Extraction. To faithfully leverage the 3D priors encoded in the generative model \mathcal{G} , we follow a feature extraction strategy

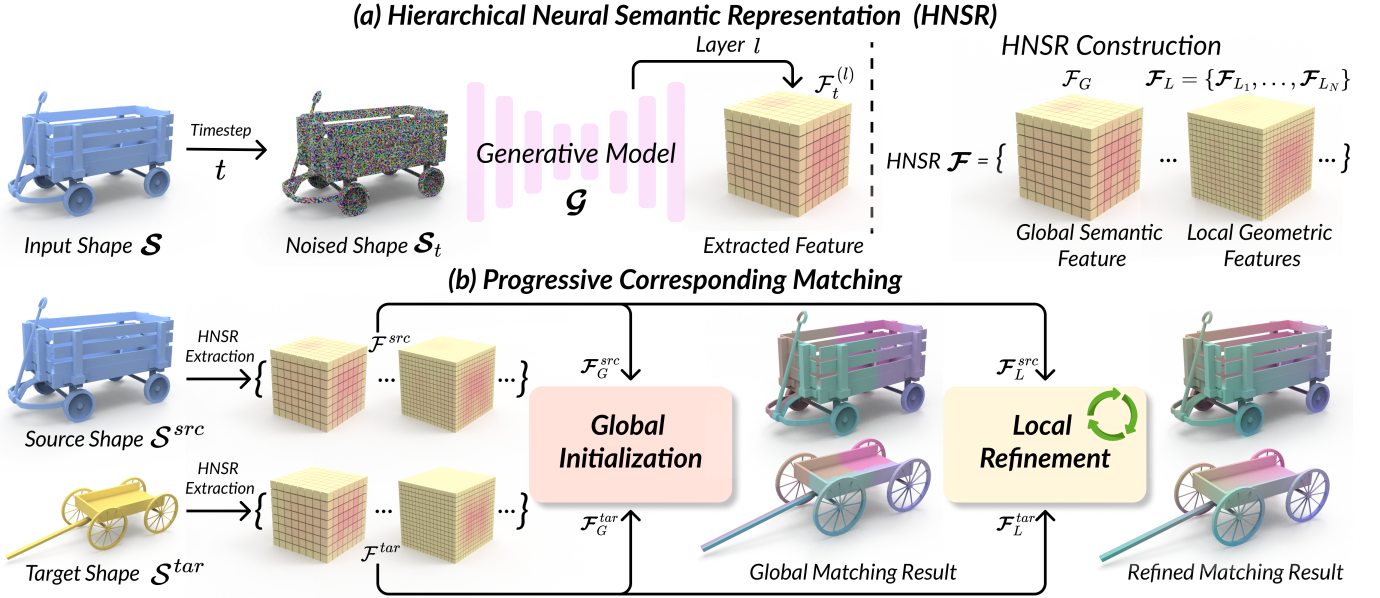


Fig. 2. Overview of our approach. (a) We design the hierarchical neural semantic representation (HNSR) using multi-scale features extracted from a pre-trained 3D generative model \mathcal{G} . Given an input shape \mathcal{S} , we add noise to obtain \mathcal{S}_t at time step t , and extract features $\mathcal{F}_t^{(l)}$ from the l -th layer of \mathcal{G} . By aggregating a global feature and fine features across multiple layers, we construct the HNSR \mathcal{F} for the input shape. (b) Given a pair of source and target shapes, we propose a progressive global-to-local matching strategy for 3D semantic correspondence. We first construct their respective HNSR representations, extracting both global semantic features and local geometric features. The global features are used to perform coarse correspondence initialization, which is then iteratively refined using the local features at higher resolutions, resulting in accurate and semantically consistent correspondences.

that mirrors the model’s training. In particular, for diffusion-based generative models, training involves denoising shapes corrupted by increasing levels of Gaussian noise. To simulate this, we perturb the input shape \mathcal{S} to obtain a noisy version \mathcal{S}_t at diffusion timestep t :

$$\mathcal{S}_t = \sqrt{\bar{\alpha}_t} \mathcal{S} + \sqrt{1 - \bar{\alpha}_t} \epsilon, \quad \epsilon \sim \mathcal{N}(0, \mathbf{I}), \quad (1)$$

where $\bar{\alpha}_t$ is a predefined noise schedule on the noise level at timestep $t \in [1, T]$. We then feed the noisy shape \mathcal{S}_t into the generative model \mathcal{G} and extract intermediate features from the selected layer l :

$$\mathcal{F}_t^{(l)} = \mathcal{G}^{(l)}(\mathcal{S}_t), \quad (2)$$

where $\mathcal{G}^{(l)}$ denotes the output of the l -th layer. Each extracted feature $\mathcal{F}_t^{(l)}$ encodes the model’s internal representation of the shape, influenced by the layer depth l . By sampling across network layers, we obtain the hierarchical representations that capture the shape’s structure across varying semantic and geometric scales.

HNSR Construction. To build a representation that incorporates both coarse semantics and fine geometric cues, we organize the extracted features into a hierarchical structure based on their associated network layers. This design is motivated by [Pan et al. 2023]: deeper layers (farther from output) in neural networks tend to encode global semantics, whereas shallower layers (closer to the output) focus more on local geometries. Therefore, we define the HNSR \mathcal{F} as comprising two components:

- **Global semantic feature \mathcal{F}_G :** a single feature extracted from a deep layer, capturing high-level semantic structure and contextual information of the shape; and

- **Local geometric features $\mathcal{F}_L = \{\mathcal{F}_{L_1}, \dots, \mathcal{F}_{L_N}\}$:** a set of features collected from multiple shallow layers, each encoding fine-grained geometric and topological details at different levels of resolution.

This hierarchical neural semantic representation, $\mathcal{F} = (\mathcal{F}_G, \mathcal{F}_L)$, yields a multi-scale representation that is both semantically meaningful and geometrically precise. The resulting HNSR \mathcal{F} is training-free, serving as an efficient and versatile representation that can be applied across various pre-trained 3D generative models.

3.3 Progressive Correspondence Matching

Given a source shape \mathcal{S}^{src} and a target shape \mathcal{S}^{tar} , we first extract their respective HNSR using the strategy described in Section 3.2: $\mathcal{F}^{src} = (\mathcal{F}_G^{src}, \mathcal{F}_L^{src})$ and $\mathcal{F}^{tar} = (\mathcal{F}_G^{tar}, \mathcal{F}_L^{tar})$. A natural idea is to directly match features using either the global or local features. However, relying solely on the global semantic features often leads to low-resolution and imprecise correspondences, as Figure 2(b) (global matching result) and Figure 3(a) illustrate. On the other hand, matching only the local geometric features can lead to incorrect results in geometrically similar regions with different semantic meanings, e.g., confusing the front and back wheels of a car due to their local appearance similarity, as Figure 3(b) illustrates.

To mitigate this issue, we introduce a progressive global-to-local matching scheme. This scheme first leverages global semantic features to establish coarse correspondences that reflect high-level semantic structural relationships, and then incrementally refines

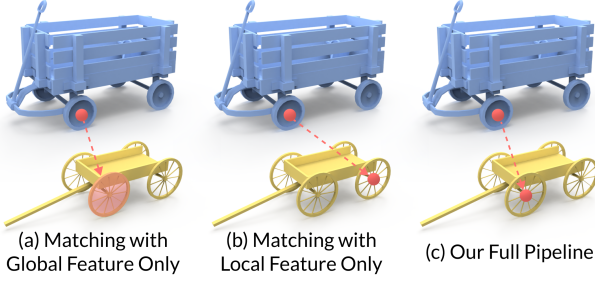


Fig. 3. Visual comparison of shape correspondence with global and local features. (a) Using global semantic features alone yields coarse alignments due to limited spatial resolution. (b) Using local geometric features alone may introduce mismatches in regions with similar local geometry but different global semantics. (c) Our progressive global-to-local matching scheme combines both, achieving correspondences that are semantically consistent and geometrically precise.

them using multi-scale local geometric features to obtain spatially-accurate correspondence, as shown in Figure 3(c). The overall matching process consists of two stages: (i) *Global Initialization*, which computes global coarse correspondences using \mathcal{F}_G^{src} and \mathcal{F}_G^{tar} ; and (ii) *Local Refinement*, which progressively improves the correspondence using the local features \mathcal{F}_L^{src} and \mathcal{F}_L^{tar} .

Global Initialization. We begin by computing a coarse semantic alignment using the global semantic features \mathcal{F}_G^{src} and \mathcal{F}_G^{tar} . For each voxel position \mathbf{v}^{src} in \mathcal{S}^{src} , we aim to identify a coarse matching region $\mathcal{R}_0^{tar} \subset \mathcal{S}^{tar}$ in the target shape that captures semantically similar content. Specifically, given the source position \mathbf{v}^{src} , we identify its corresponding position \mathbf{v}_G^{src} in the source global feature grid \mathcal{F}_G^{src} , which typically has lower spatial resolution than \mathcal{S}^{src} due to downsampling in the generative model. This mapping is computed by dividing the voxel coordinates by the resolution scale factor, depending on the feature resolution. To find a semantically similar region in the target shape, we compare the global feature at position \mathbf{v}_G^{src} with all feature vectors in the target global feature grid \mathcal{F}_G^{tar} based on cosine similarity. Specifically, for each spatial position \mathbf{v} in the target global feature grid \mathcal{F}_G^{tar} , we compute the cosine similarity between the source feature vector $\mathcal{F}_G^{src}[\mathbf{v}_G^{src}]$ and the target feature vector $\mathcal{F}_G^{tar}[\mathbf{v}]$. The most semantically similar position \mathbf{v}_G^{tar} is then selected as follows:

$$\mathbf{v}_G^{tar} = \arg \min_{\mathbf{v} \in \mathcal{F}_G^{tar}} \delta_{\cos}(\mathcal{F}_G^{src}[\mathbf{v}_G^{src}], \mathcal{F}_G^{tar}[\mathbf{v}]), \quad (3)$$

where $\delta_{\cos}(\cdot, \cdot)$ denotes cosine similarity. Since the global feature grid \mathcal{F}_G^{tar} is defined at a lower resolution than the voxel grid \mathcal{S}^{tar} , the matched position \mathbf{v}_G^{tar} corresponds to a coarse region in \mathcal{S}^{tar} . Therefore, we map \mathbf{v}_G^{tar} back to the coarse region $\mathcal{R}_0^{tar} \subset \mathcal{S}^{tar}$ by upsampling. This establishes a global mapping, where each voxel position \mathbf{v}^{src} in \mathcal{S}^{src} is associated with a corresponding region \mathcal{R}_0^{tar} in the target shape. This region serves as a semantic prior to guide the subsequent local refinement process.

Local Refinement. In this stage, given a source voxel position \mathbf{v}^{src} in \mathcal{S}^{src} and its corresponding coarse semantic region $\mathcal{R}_0^{tar} \subset \mathcal{S}^{tar}$ obtained from the global initialization stage, our goal is to progressively refine this region using the local geometric features. Specifically, we utilize the local features $\mathcal{F}_L = \{\mathcal{F}_{L_1}, \dots, \mathcal{F}_{L_N}\}$ to obtain

a sequence of increasingly precise regions $\{\mathcal{R}_i^{tar} | \mathcal{R}_i^{tar} \subset \mathcal{R}_{i-1}^{tar} \subset \mathcal{S}^{tar}$ and $i \in [1, N]\}$. This progressive refinement ultimately yields an accurate corresponding position \mathbf{v}^{tar} in \mathcal{S}^{tar} . At each refinement level i , we first downsample the voxel coordinates in \mathcal{R}_{i-1}^{tar} to match the resolution of the target local feature $\mathcal{F}_{L_i}^{tar}$. This produces a restricted index set \mathcal{A}_i^{tar} within the spatial domain of $\mathcal{F}_{L_i}^{tar}$, which serves as the candidate search region at level i . For the voxel position \mathbf{v}^{src} in \mathcal{S}^{src} , we downsample its coordinate to obtain \mathbf{v}_i^{src} in the source's local feature grid $\mathcal{F}_{L_i}^{src}$ and extract its corresponding feature vector $\mathcal{F}_{L_i}^{src}[\mathbf{v}_i^{src}]$. We then identify the best matching position in the restricted target region according to the cosine similarity:

$$\mathbf{v}_i^{tar} = \arg \min_{\mathbf{v} \in \mathcal{A}_i^{tar}} \delta_{\cos}(\mathcal{F}_{L_i}^{src}[\mathbf{v}_i^{src}], \mathcal{F}_{L_i}^{tar}[\mathbf{v}]). \quad (4)$$

where position \mathbf{v}_i^{tar} corresponds to a voxel in $\mathcal{F}_{L_i}^{tar}$, from which we upsample back to \mathcal{S}^{tar} to define a finer region $\mathcal{R}_i^{tar} \subset \mathcal{R}_{i-1}^{tar} \subset \mathcal{S}^{tar}$. This region is then used as input for the next refinement level. Repeating this process over all levels N times enables us to obtain progressively refined correspondence positions, ultimately leading to more accurate correspondence between the source and target shapes. While local refinement depends on global initialization, the global stage typically provides rough but robust correspondences, avoiding failures from bad global initialization.

3.4 Backbones for Neural Semantic Representation

Our neural semantic representation extraction framework is designed to work with diverse pre-trained 3D generative models, even though the form of the input shape \mathcal{S} and the structure of the generator \mathcal{G} vary across different backbones. In this section, we describe three representative backbones that can be incorporated in our framework and clarify how \mathcal{S} and \mathcal{G} are defined in each case.

SDF-Diffusion [Shim et al. 2023]: The input shape \mathcal{S} is represented as a voxelized signed distance field (SDF) volume at a resolution of 32^3 , where each voxel encodes the signed distance to the shape surface. The generative model \mathcal{G} is a U-Net-based diffusion model trained to synthesize such SDF volumes via iterative denoising. While SDF-Diffusion further employs a separate super-resolution module to upsample the generated SDFs into high-resolution outputs, this module is not involved in our NSR extraction process.

LAS-Diffusion [Zheng et al. 2023]: \mathcal{S} is a $64 \times 64 \times 64$ binary occupancy grid. The generator \mathcal{G} is a U-Net-based diffusion model trained to generate shapes represented as occupancy grids via iterative denoising, which forms the first stage of the LAS-Diffusion pipeline. The second stage is a separate super-resolution module that refines the coarse shape into a high-quality signed distance field (SDF), but it is not involved in our NSR extraction.

TRELLIS [Xiang et al. 2025]: \mathcal{S} is a voxel structural embedding at a resolution of 16^3 , representing the geometry of the input shape. TRELLIS utilizes multi-view image features to construct a structured latent representation (SLAT) through a two-stage rectified flow process: first predicting a voxel structure embedding \mathcal{S} , capturing geometry structure, then generating fine-grained latent codes. The generator \mathcal{G} refers to the first stage that produces \mathcal{S} . Specifically, we adopt the stage-one voxel embeddings, which provide

Table 1. Accuracy and error comparison for shape correspondence. We report the accuracy within a 1% error tolerance, comparing our method with previous works. “–” denotes unavailable results. The best and second-best results are highlighted in **bold** and underlined. Since 3D-CODED [Groueix et al. 2018] does not offer a pre-trained model for the SHREC’ 20 dataset, a comparison with this method is not provided in this dataset.

Methods	SHREC’ 19		SHREC’ 20	
	Accuracy \uparrow	Error \downarrow	Accuracy \uparrow	Error \downarrow
DPC	17.4	6.3	31.1	2.1
SE-ORNet	21.4	4.6	31.7	1.0
3D-CODED	2.1	8.1	–	–
FM + WKS	4.4	3.3	4.1	7.3
DenseMatcher	11.3	6.5	27.8	2.7
DIFF3F	<u>26.4</u>	1.7	<u>72.6</u>	0.9
DIFF3F + FM	21.6	<u>1.5</u>	62.3	<u>0.7</u>
HSNR (Ours)	37.4	1.3	83.8	0.5

Table 2. Comparing geodesic error and edge distortion ratio for shape correspondence. Notice that our method consistently achieves the best results (lowest geodesic error and edge distortion ratio closer to one) for all cases. The units of the geodesic error is 10^{-3} .

Methods	SHREC’ 19		SHREC’ 20	
	Error \downarrow	Ratio ~ 1	Error \downarrow	Ratio ~ 1
DenseMatcher	96	1.62	33	1.43
DIFF3F	21	1.36	11	1.14
HSNR (Ours)	15	1.24	6	1.11

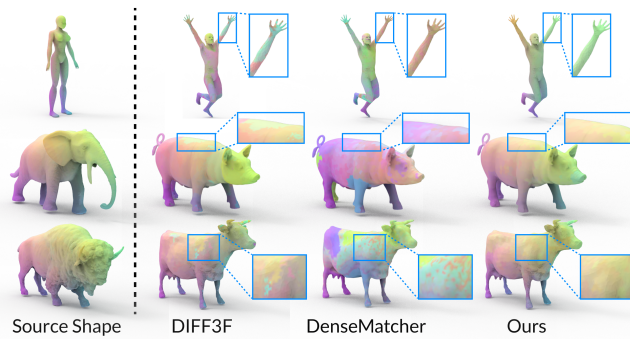


Fig. 4. Visual comparison with the state-of-the-art methods DIFF3F [Dutt et al. 2024] and DenseMatcher [Zhu et al. 2024]. Our method produces more accurate and coherent correspondences, while the results from DIFF3F and DenseMatcher are noisier and less consistent.

a volumetric representation naturally suited to our voxel-based pipeline, whereas the stage-two sparse codes are less compatible.

4 RESULTS AND EXPERIMENTS

4.1 Datasets and Implementation Details

Evaluations include six benchmark datasets: ShapeNet [Chang et al. 2015], ShapeNet Part [Yi et al. 2016], Objaverse [Deitke et al. 2023b], Objaverse(XL) [Deitke et al. 2023a], SHREC’19 [Melzi et al. 2019], and SHREC’20 [Dyke et al. 2020]. We adapt our approach to three

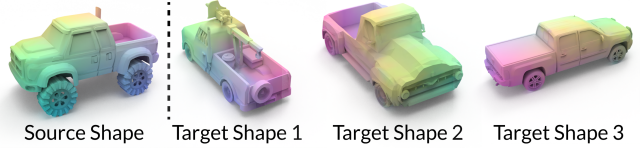


Fig. 5. Visual correspondence results on shapes with different orientations. By leveraging TRELLIS [Xiang et al. 2025], our method can produce meaningful correspondences even if the shapes are not canonically aligned.

different pre-trained generative backbones: SDF-Diffusion [Shim et al. 2023], LAS-Diffusion [Zheng et al. 2023], and TRELLIS [Xiang et al. 2025]. Regarding inference efficiency, we report the average runtime over 10 shape pairs: SDF-Diffusion, LAS-Diffusion, and TRELLIS take 1.6, 1.3, and 2.8 seconds per pair, respectively. For SDF-Diffusion and LAS-Diffusion, the global semantic feature \mathcal{F}_G is extracted from the 1st layer of the generator’s decoder, whereas the local geometric features \mathcal{F}_L are obtained from the 2nd and 3rd layers. For TRELLIS, \mathcal{F}_G is extracted from the 4th layer of the generator and the local geometric features \mathcal{F}_L are taken from the 6th, 8th, and 10th layers. The diffusion timestep t is set to 45 for LAS-Diffusion, 50 for SDF-Diffusion, and 12 for TRELLIS.

4.2 Experimental Settings

To evaluate the effectiveness of our method, we compare it with various baselines on both shape correspondence and co-segmentation.

Shape correspondence. We compare our approach with DPC [Lang et al. 2021], SE-ORNet [Deng et al. 2023], 3D-CODED [Groueix et al. 2018], FM+WKS [Ovsjanikov et al. 2012], DenseMatcher [Zhu et al. 2024], and DIFF3F [Dutt et al. 2024]. Following [Deng et al. 2023; Dutt et al. 2024], we evaluate on both SHREC’19 [Melzi et al. 2019] (44 human scans with 430 annotated test pairs) and SHREC’20 [Dyke et al. 2020] (featuring animals in diverse poses with expert-labeled non-isometric correspondences). We evaluate correspondence accuracy using the provided ground-truth annotations.

Shape co-segmentation. We compare our method with various baselines: BAE-Net [Chen et al. 2019], RIM-Net [Niu et al. 2022], SATR [Abdelreheem et al. 2023b], DAE-Net [Chen et al. 2024], and DenseMatcher [Zhu et al. 2024]. Following [Chen et al. 2019], we evaluate shape on ShapeNet Part [Yi et al. 2016], focusing on the following 13 categories: airplane, cap, chair, earphone, guitar, knife, lamp, motorbike, mug, pistol, rocket, skateboard, and table. In our setting, co-segmentation is performed by transferring part labels from a labeled source shape to an unlabeled target shape. For each position on the target shape, we estimate its corresponding location on the source shape using our correspondence method, and then assign the part label from the source to the target.

4.3 Quantitative Comparison

Evaluation metrics. We evaluate correspondence estimation using two standard metrics, following [Dutt et al. 2024]: average correspondence error and correspondence accuracy. Besides, we report two conventional metrics, *i.e.*, average geodesic distance and edge distortion ratio, to assess the accuracy and smoothness of the correspondences. For co-segmentation, we follow [Chen et al. 2019]

Table 3. Per-part IoU comparison on the co-segmentation task. The best and second-best results are marked in **bold** and underlined. Our method with all three backbones consistently outperforms the state-of-the-art method across all categories, demonstrating the effectiveness and robustness of our framework.

Methods	plane	cap	chair	earphone	guitar	knife	lamp	motorbike	mug	pistol	rocket	skateboard	table	average
BAE-Net	67.8	82.1	66.5	52.1	53.9	41.5	75.3	23.1	95.3	31.4	42.1	65.7	76.5	60.7
RIM-Net	61.9	59.3	75.7	70.8	46.3	40.7	60.6	28.7	67.6	36.9	36.7	65.9	71.4	53.1
SATR	40.6	22.9	58.3	22.6	50.6	53.7	47.6	16.6	54.3	23.3	36.7	48.9	37.5	42.1
DAE-Net	76.3	82.4	82.3	76.9	88.1	82.1	73.2	48.4	95.6	73.2	38.7	69.2	74.5	74.7
DenseMatcher	52.1	42.5	63.2	35.9	54.1	41.9	62.3	19.8	68.4	20.8	41.2	58.0	63.2	48.2
HNSR + SDF-Diffusion	63.1	80.4	71.7	80.7	89.2	79.5	77.3	<u>56.7</u>	96.7	<u>83.7</u>	46.4	80.9	70.0	75.8
HNSR + LAS-Diffusion	79.4	84.1	86.0	80.6	<u>90.3</u>	<u>83.9</u>	83.8	62.6	<u>96.5</u>	<u>83.2</u>	60.2	81.9	<u>88.3</u>	82.7
HNSR + TRELLIS	<u>77.5</u>	<u>83.6</u>	<u>83.1</u>	77.4	90.6	85.8	<u>81.2</u>	51.2	95.1	85.7	<u>57.8</u>	<u>81.2</u>	<u>89.2</u>	81.0

and report per-part IoU, averaged over all parts and shapes in each category. Please see Supplementary material Section A for details.

Table 1 reports the quantitative results on correspondence estimation. As SDF-Diffusion and LAS-Diffusion are not trained on human/animal shapes, we evaluate only the TRELLIS backbone on SHREC’19 and SHREC’20. Without additional training, our method outperforms prior approaches across all metrics, demonstrating its effectiveness. Table 2 reports the quantitative results on geodesic accuracy error and smoothness estimation. Here, we evaluate the TRELLIS backbone on SHREC’19 and SHREC’20. Again, even without additional training, our method surpasses prior approaches in both metrics. Table 3 presents the results on co-segmentation. Our method with different backbones consistently outperforms state-of-the-art methods for all categories on all metrics, showing the robustness and generalizability of our framework design.

4.4 Qualitative Comparison

Shape correspondence. We provide visual comparisons of our method with state-of-the-art approaches DIFF3F [Dutt et al. 2024] and DenseMatcher [Zhu et al. 2024], which are the most relevant to ours—both methods establish 3D correspondences by utilizing 2D image features. Figure 4 shows qualitative comparisons with DIFF3F and DenseMatcher. Our method yields more accurate correspondences on both human and animal shapes, whereas DIFF3F and DenseMatcher tend to produce noticeably noise in results. This comparison reveals the domain gap between 2D and 3D representations, further showing the effectiveness of our 3D-native approach.

Shape co-segmentation. Figure 8 presents visual comparisons of our method with existing baselines on co-segmentation. For all three 3D generative backbones, our framework consistently produces more precise parts co-segmentation with clear and well-aligned boundaries. As the third row of Figure 8 shows, our method is able to co-segment all the four legs as distinct parts. In contrast, baseline methods tend to merge these substructures.

More visual comparison results on shape correspondence and co-segmentation are shown in Supplementary Sections B and C.

4.5 More Visual Results

Figures 6 and 9 present additional qualitative results of correspondence and co-segmentation produced by our approach. These results are generated using TRELLIS [Xiang et al. 2025], as it is trained on Objaverse and thus supports evaluation on more diverse shapes.

Further, since Objaverse contains unaligned shapes with varying orientations, TRELLIS learns to capture pose and orientation variations during training. Though our method does not explicitly

consider rotation invariance, we observe that it appears to inherit this property of TRELLIS to establish correspondences, even when the source and target shapes have different orientations; see Figure 5. More visual results on shape correspondence and co-segmentation are shown in Sections D and E of the supplementary materials.

4.6 Applications

Leveraging the estimated correspondences, our method enables faithful texture transfer and keypoint matching across diverse 3D shapes. As Figure 7 (right) shows, texture patterns are preserved and aligned consistently with the corresponding semantic regions. To achieve this, our method leverages the part-wise UV maps available in Objaverse [Deitke et al. 2023a]. Given a source mesh and a target mesh, we first establish semantic correspondences between their respective parts using our approach. Then, for each matched part pair, we map the texture from the source part’s UV map to the UV coordinates of the corresponding target part. This part-level transfer ensures semantic alignment and appearance consistency.

Figure 7 (left) shows our keypoint matching results. Given a user-specified keypoint on the source shape, our framework is able to automatically locate the semantically corresponding position on the target shapes via the estimated semantic correspondence. The results remain consistent and accurate for diverse geometries and categories. From the third row of Figure 7 (left), we can see that when a keypoint is placed on a human foot, our method can correctly transfer it to the corresponding position of a deer, demonstrating our method’s robust cross-category semantic-matching capabilities. See Supplementary Section F for more visual results.

4.7 Ablation Studies

Due to page limit, see Supplementary Section G for ablation studies.

5 CONCLUSION

We presented a new framework, namely hierarchical neural semantic representation (HNSR), for 3D semantic correspondence by leveraging features extracted from pre-trained 3D generative models. In summary, hierarchical neural semantic representation is a multiresolution representation composed of global semantic features and local geometric features, designed to capture both high-level structural context and fine-grained geometric details. Further equipped with the progressive global-to-local matching strategy, our framework is able to construct accurate and semantically consistent correspondence, without requiring additional training. Our approach demonstrates strong generalization across diverse shape

categories and topologies, achieving state-of-the-art performance on standard benchmarks for correspondence estimation and shape co-segmentation. Moreover, we showcase its utility in real-world applications such as texture transfer and keypoint matching, highlighting its robustness and versatility.

Limitations and Future Work. While our method shows strong performance in estimating semantic correspondences for a wide variety of 3D objects, its effectiveness inherently depends on the capability of the pre-trained generative model. If a target shape lies far outside the training distribution of the generative prior, the extracted features may not be able to encode meaningful semantics or geometric cues, leading to degraded correspondence performance. Although our approach demonstrates generalization to diverse categories using foundation models like TRELLIS, domain shifts or underrepresented categories can still pose challenges. A potential research direction is to enhance the robustness of generative models by incorporating additional fine-tuning process.

Moreover, our current framework is designed for static shape pairs. While we demonstrate successful transfer across category and topology, the framework does not directly address correspondences in time-varying shape sequences. Extending our approach to support temporally consistent correspondence in dynamic 4D datasets would be a promising and impactful direction. For instance, tracking the foot region across frames in a sequence, where both a human and a deer are running, requires maintaining semantic consistency over time, despite continuous deformation and pose variation. Incorporating spatiotemporal priors could help capture such dynamics, paving the way for robust and temporally stable correspondence estimation in complex real-world scenarios.

References

Ahmed Abdelreheem, Abdelrahman Eldeesokey, Maks Ovsjanikov, and Peter Wonka. 2023a. Zero-shot 3D Shape Correspondence. In *Proceedings of SIGGRAPH Asia*. 1–11.

Ahmed Abdelreheem, Ivan Skorokhodov, Maks Ovsjanikov, and Peter Wonka. 2023b. SATR: Zero-shot Semantic Segmentation of 3D Shapes. In *IEEE Conference on Computer Vision and Pattern Recognition (CVPR)*. 15166–15179.

Herbert Bay, Tinne Tuytelaars, and Luc Van Gool. 2006. SURF: Speeded Up Robust Features. In *European Conference on Computer Vision (ECCV)*. 404–417.

Alexander M Bronstein, Michael M Bronstein, and Ron Kimmel. 2008. *Numerical Geometry of Non-rigid Shapes*. Springer Science & Business Media.

Dongliang Cao and Florian Bernard. 2023. Self-supervised Learning for Multimodal Non-rigid 3D Shape Matching. In *IEEE Conference on Computer Vision and Pattern Recognition (CVPR)*. 17735–17744.

Angel X. Chang, Thomas Funkhouser, Leonidas J. Guibas, Pat Hanrahan, Qixing Huang, Zimo Li, Silvio Savarese, Manolis Savva, Shuran Song, Hao Su, et al. 2015. ShapeNet: An Information-Rich 3D Model Repository. *arXiv preprint arXiv:1512.03012* (2015).

Zhiqin Chen, Qimin Chen, Hang Zhou, and Hao Zhang. 2024. DAE-Net: Deforming Auto-Encoder for Fine-grained Shape Co-segmentation. In *Proceedings of SIGGRAPH*. 1–11.

Zhiqin Chen, Kangxue Yin, Matthew Fisher, Siddhartha Chaudhuri, and Hao Zhang. 2019. BAE-Net: Branched Autoencoder for Shape Co-segmentation. In *IEEE International Conference on Computer Vision (ICCV)*. 8490–8499.

Matt Deitke, Ruoshi Liu, Matthew Wallingford, Huong Ngo, Oscar Michel, Aditya Kusupati, Alan Fan, Christian Laforte, Vikram Voleti, Samir Yitzhak Gadre, et al. 2023a. Objaverse-XL: A Universe of 10M+ 3D Objects. *arXiv preprint arXiv:2307.05663* (2023).

Matt Deitke, Dustin Schwenk, Jordi Salvador, Luca Weihs, Oscar Michel, Eli VanderBilt, Ludwig Schmidt, Kiana Ehsani, Aniruddha Kembhavi, and Ali Farhadi. 2023b. Objaverse: A Universe of Annotated 3D Objects. In *IEEE Conference on Computer Vision and Pattern Recognition (CVPR)*. 13142–13153.

Jiacheng Deng, Chuxin Wang, Jiahao Lu, Jianfeng He, Tianzhu Zhang, Jiyang Yu, and Zhe Zhang. 2023. SE-ORNet: Self-Ensembling Orientation-aware Network for Unsupervised Point Cloud Shape Correspondence. In *IEEE Conference on Computer Vision and Pattern Recognition (CVPR)*. 5364–5373.

Yu Deng, Jiaolong Yang, and Xin Tong. 2021. Deformed Implicit Field: Modeling 3D Shapes with Learned Dense Correspondence. In *IEEE Conference on Computer Vision and Pattern Recognition (CVPR)*. 10286–10296.

Huong Quynh Dinh, Anthony Yezzi, and Greg Turk. 2005. Texture Transfer during Shape Transformation. *ACM Transactions on Graphics* 24, 2 (2005), 289–310.

Nicolas Donati, Abhishek Sharma, and Maks Ovsjanikov. 2020. Deep Geometric Functional Maps: Robust Feature Learning for Shape Correspondence. In *IEEE Conference on Computer Vision and Pattern Recognition (CVPR)*. 8592–8601.

Niladri Shekhar Dutt, Sanjeev Muralikrishnan, and Niloy J. Mitra. 2024. Diffusion 3D Features (Diff3F): Decorating Untextured Shapes with Distilled Semantic Features. In *IEEE Conference on Computer Vision and Pattern Recognition (CVPR)*. 4494–4504.

Roberto M Dyke, Yu-Kun Lai, Paul L Rosin, Stefano Zappalà, Seana Dykes, Daoliang Guo, Kun Li, Riccardo Marin, Simone Melzi, and Jingyu Yang. 2020. SHREC’20: Shape Correspondence with Non-Isometric Deformations. *Computers & Graphics* 92 (2020), 28–43.

Marvin Eisenberger, Zorah Lähner, and Daniel Cremers. 2019. Divergence-Free Shape Correspondence by Deformation. In *Computer Graphics Forum*, Vol. 38. 1–12.

Marvin Eisenberger, Zorah Lahner, and Daniel Cremers. 2020. Smooth Shells: Multi-scale Shape Registration with Functional Maps. In *IEEE Conference on Computer Vision and Pattern Recognition (CVPR)*. 12265–12274.

Ian Goodfellow, Jean Pouget-Abadie, Mehdi Mirza, Bing Xu, David Warde-Farley, Sherjil Ozair, Aaron Courville, and Yoshua Bengio. 2014. Generative Adversarial Nets. In *Conference on Neural Information Processing Systems (NeurIPS)*. 2672–2680.

Thibault Groueix, Matthew Fisher, Vladimír G Kim, Bryan C Russell, and Mathieu Aubry. 2018. 3D-CODED: 3D Correspondences by Deep Deformation. In *European Conference on Computer Vision (ECCV)*. 230–246.

Oshri Halimi, Or Litany, Emanuele Rodola, Alex M Bronstein, and Ron Kimmel. 2019. Unsupervised Learning of Dense Shape Correspondence. In *Proceedings of the IEEE/CVF Conference on Computer Vision and Pattern Recognition*. 4370–4379.

Jonathan Ho, Ajay Jain, and Pieter Abbeel. 2020. Denoising Diffusion Probabilistic Models. *Conference on Neural Information Processing Systems (NeurIPS)* (2020), 6840–6851.

Fangzhou Hong, Jiaxiang Tang, Ziang Cao, Min Shi, Tong Wu, Zhaoxi Chen, Tengfei Wang, Liang Pan, Dahua Lin, and Ziwei Liu. 2024. 3DTopia: Large Text-to-3D Generation Model with Hybrid Diffusion Priors. *arXiv preprint arXiv:2403.02234* (2024).

Qixing Huang, Fan Wang, and Leonidas Guibas. 2014. Functional Map Networks for Analyzing and Exploring Large Shape Collections. *ACM Transactions on Graphics* 33, 4 (2014), 1–11.

Qi-Xing Huang, Bart Adams, Martin Wicke, and Leonidas J Guibas. 2008. Non-Rigid Registration Under Isometric Deformations. In *Computer Graphics Forum*, Vol. 27. 1449–1457.

Ka-Hei Hui, Aditya Sanghi, Arianna Rampini, Kamal Rahimi Malekshan, Zhengzhe Liu, Hooman Shayan, and Chi-Wing Fu. 2024. Make-A-Shape: A Ten-Million-Scale 3D Shape Model. In *Proceedings of International Conference on Machine Learning (ICML)*.

Wei Jiang, Eduard Trulls, Jan Hosang, Andrea Tagliasacchi, and Kwang Moo Yi. 2021. COTR: Correspondence Transformer for Matching across Images. In *IEEE Conference on Computer Vision and Pattern Recognition (CVPR)*. 6207–6217.

Yuhe Jin, Dmytro Mishkin, Anastasia Mishchuk, Jiri Matas, Pascal Fua, Kwang Moo Yi, and Eduard Trulls. 2021. Image Matching across Wide Baselines: From Paper to Practice. *International Journal of Computer Vision* 129, 2 (2021), 517–547.

Vladimir G Kim, Yaron Lipman, and Thomas Funkhouser. 2011. Blended Intrinsic Maps. *ACM Transactions on Graphics* 30, 4 (2011), 1–12.

Artiom Kovnatsky, Michael M Bronstein, Xavier Bresson, and Pierre Vandergheynst. 2015. Functional Correspondence by Matrix Completion. In *IEEE Conference on Computer Vision and Pattern Recognition (CVPR)*. 905–914.

Itai Lang, Dvir Ginzburg, Shah Avidan, and Dan Raviv. 2021. DPC: Unsupervised Deep Point Correspondence via Cross and Self Construction. In *2021 International Conference on 3D Vision (3DV)*. 1442–1451.

Jae Yong Lee, Joseph DeGol, Victor Fragoso, and Sudipta N Sinha. 2021. Patchmatch-Based Neighborhood Consensus for Semantic Correspondence. In *IEEE Conference on Computer Vision and Pattern Recognition (CVPR)*. 13153–13163.

Yangguang Li, Zi-Xin Zou, Zexiang Liu, Dehu Wang, Yuan Liang, Zhipeng Yu, Xingchao Liu, Yuan-Chen Guo, Ding Liang, Wanli Ouyang, et al. 2025. TripoSG: High-Fidelity 3D Shape Synthesis using Large-Scale Rectified Flow Models. *arXiv preprint arXiv:2502.06608* (2025).

Or Litany, Tal Remez, Emanuele Rodola, Alex Bronstein, and Michael Bronstein. 2017a. Deep Functional Maps: Structured Prediction for Dense Shape Correspondence. In *IEEE International Conference on Computer Vision (ICCV)*. 5659–5667.

Or Litany, Emanuele Rodolà, Alexander M Bronstein, and Michael M Bronstein. 2017b. Fully Spectral Partial Shape Matching. In *Computer Graphics Forum*, Vol. 36. 247–258.

Haolin Liu, Xiaohang Zhan, Zizheng Yan, Zhongjin Luo, Yuxin Wen, and Xiaoguang Han. 2025. Stable-SCore: A stable registration-based framework for 3d shape correspondence. In *IEEE Conference on Computer Vision and Pattern Recognition (CVPR)*. 917–928.

David G Lowe. 2004. Distinctive Image Features from Scale-Invariant Keypoints. *International Journal of Computer Vision* 60 (2004), 91–110.

Grace Luo, Lisa Dunlap, Dong Huk Park, Aleksander Holynski, and Trevor Darrell. 2023. Diffusion Hyperfeatures: Searching Through Time and Space for Semantic Correspondence. In *Conference on Neural Information Processing Systems (NeurIPS)*, Vol. 36. 47500–47510.

Riccardo Marin, Marie-Julie Rakotosaona, Simone Melzi, and Maks Ovsjanikov. 2020. Correspondence Learning via Linearly-Invariant Embedding. *Conference on Neural Information Processing Systems (NeurIPS)* 33, 1608–1620.

Simone Melzi, Riccardo Marin, Emanuele Rodolà, Umberto Castellani, Jing Ren, Adrien Poulenard, P Ovsjanikov, et al. 2019. SHREC’19: Matching Humans with Different Connectivity. In *Eurographics Workshop on 3D Object Retrieval*. The Eurographics Association, 1–8.

Juhong Min, Jongmin Lee, Jean Ponce, and Minsu Cho. 2020. Learning to Compose Hypercolumns for Visual Correspondence. In *European Conference on Computer Vision (ECCV)*. 346–363.

Chengjie Niu, Manyi Li, Kai Xu, and Hao Zhang. 2022. RIM-Net: Recursive Implicit Fields for Unsupervised Learning of Hierarchical Shape Structures. In *IEEE Conference on Computer Vision and Pattern Recognition (CVPR)*. 11779–11788.

Dorian Nogneng and Maks Ovsjanikov. 2017. Informative Descriptor Preservation via Commutativity for Shape Matching. In *Computer Graphics Forum*, Vol. 36. 259–267.

Maks Ovsjanikov, Mirela Ben-Chen, Justin Solomon, Adrian Butscher, and Leonidas Guibas. 2012. Functional Maps: A Flexible Representation of Maps between Shapes. *ACM Transactions on Graphics* 31, 4 (2012), 11 pages.

Xingang Pan, Ayush Tewari, Thomas Leimkühler, Lingjie Liu, Abhimitra Meka, and Christian Theobalt. 2023. Drag Your GAN: Interactive Point-Based Manipulation on the Generative Image Manifold. In *Proceedings of SIGGRAPH*. 1–11.

William Peebles, Jun-Yan Zhu, Richard Zhang, Antonio Torralba, Alexei A Efros, and Eli Shechtman. 2022. GAN-Supervised Dense Visual Alignment. In *IEEE Conference on Computer Vision and Pattern Recognition (CVPR)*. 13470–13481.

Jing Ren, Mikhail Panine, Peter Wonka, and Maks Ovsjanikov. 2019. Structured Regularization of Functional Map Computations. In *Computer Graphics Forum*, Vol. 38. 39–53.

Jing Ren, Adrien Poulenard, Peter Wonka, and Maks Ovsjanikov. 2018. Continuous and Orientation-Preserving Correspondences via Functional Maps. *ACM Transactions on Graphics* 37, 6 (2018), 1–16.

Ignacio Rocco, Relja Arandjelović, and Josef Sivic. 2018. End-to-End Weakly-Supervised Semantic Alignment. In *IEEE Conference on Computer Vision and Pattern Recognition (CVPR)*. 6917–6925.

Emanuele Rodola, Samuel Rota Bulo, Thomas Windheuser, Matthias Vestner, and Daniel Cremers. 2014. Dense Non-Rigid Shape Correspondence using Random Forests. In *IEEE Conference on Computer Vision and Pattern Recognition (CVPR)*. 4177–4184.

Jean-Michel Roufosse, Abhishek Sharma, and Maks Ovsjanikov. 2019. Unsupervised Deep Learning for Structured Shape Matching. In *IEEE Conference on Computer Vision and Pattern Recognition (CVPR)*. 1617–1627.

Abhishek Sharma and Maks Ovsjanikov. 2020. Weakly Supervised Deep Functional Maps for Shape Matching. In *Conference on Neural Information Processing Systems (NeurIPS)*. 19264–19275.

Jaehyeok Shim, Changwoo Kang, and Kyungdon Joo. 2023. Diffusion-Based Signed Distance Fields for 3D Shape Generation. In *IEEE Conference on Computer Vision and Pattern Recognition (CVPR)*. 20887–20897.

Oana Sidi, Oliver Van Kaick, Yanir Kleiman, Hao Zhang, and Daniel Cohen-Or. 2011. Unsupervised Co-segmentation of a Set of Shapes via Descriptor-Space Spectral Clustering. *ACM Transactions on Graphics (SIGGRAPH Asia)* (2011), 1–10.

Robert W Sumner and Jovan Popović. 2004. Deformation Transfer for Triangle Meshes. *ACM Transactions on Graphics* 23, 3 (2004), 399–405.

Mingze Sun, Chen Guo, Puhua Jiang, Shiwei Mao, Yurun Chen, and Ruqi Huang. 2024. SRIF: Semantic shape registration empowered by diffusion-based image morphing and flow estimation. In *Proceedings of SIGGRAPH Asia*. 1–11.

Luming Tang, Menglin Jia, Qianqian Wang, Cheng Perng Phoo, and Bharath Hariharan. 2023. Emergent Correspondence from Image Diffusion. In *Conference on Neural Information Processing Systems (NeurIPS)*, Vol. 36. 1363–1389.

Oliver Van Kaick, Hao Zhang, Ghassan Hamarneh, and Daniel Cohen-Or. 2011. A Survey on Shape Correspondence. In *Computer graphics forum*, Vol. 30. 1681–1707.

Jianfeng Xiang, Zelong Lv, Sicheng Xu, Yu Deng, Ruicheng Wang, Bowen Zhang, Dong Chen, Xin Tong, and Jiaolong Yang. 2025. Structured 3D Latents for Scalable and Versatile 3D Generation. In *IEEE Conference on Computer Vision and Pattern Recognition (CVPR)*. 1–10.

Li Yi, Vladimir G Kim, Duygu Ceylan, I-Chao Shen, Mengyan Yan, Hao Su, Cewu Lu, Qixing Huang, Alla Sheffer, and Leonidas Guibas. 2016. A Scalable Active Framework for Region Annotation in 3D Shape Collections. *ACM Transactions on Graphics* 35, 6 (2016), 1–12.

Hao Zhang, Alla Sheffer, Daniel Cohen-Or, Quan Zhou, Oliver Van Kaick, and Andrea Tagliasacchi. 2008. Deformation-Driven Shape Correspondence. In *Computer Graphics Forum*, Vol. 27. 1431–1439.

Junyi Zhang, Charles Herrmann, Junhwa Hur, Luisa Polania Cabrera, Varun Jampani, Dqing Sun, and Ming-Hsuan Yang. 2023. A Tale of Two Features: Stable Diffusion Complements Dino for Zero-shot Semantic Correspondence. In *Conference on Neural Information Processing Systems (NeurIPS)*, Vol. 36. 45533–45547.

Longwen Zhang, Ziyu Wang, Qixuan Zhang, Qiwei Qiu, Anqi Pang, Haoran Jiang, Wei Yang, Lan Xu, and Jingyi Yu. 2024. CLAY: A Controllable Large-scale Generative Model for Creating High-quality 3D Assets. *ACM Transactions on Graphics (SIGGRAPH)* 43, 4 (2024), 1–20.

Yuxuan Zhang, Huan Ling, Jun Gao, Kangxue Yin, Jean-Francois Lafleche, Adela Barriuso, Antonio Torralba, and Sanja Fidler. 2021. DatasetGAN: Efficient Labeled Data Factory with Minimal Human Effort. In *IEEE Conference on Computer Vision and Pattern Recognition (CVPR)*. 10145–10155.

Zibo Zhao, Zeqiang Lai, Qingxiang Lin, Yunfei Zhao, Haolin Liu, Shuhui Yang, Yifei Feng, Mingxin Yang, Sheng Zhang, Xianghui Yang, et al. 2025. Hunyuan3D 2.0: Scaling Diffusion Models for High Resolution Textured 3D Assets Generation. *arXiv preprint arXiv:2501.12202* (2025).

Xin-Yang Zheng, Hao Pan, Peng-Shuai Wang, Xin Tong, Yang Liu, and Heung-Yeung Shum. 2023. Locally Attentional SDF Diffusion for Controllable 3D Shape Generation. *ACM Transactions on Graphics (SIGGRAPH)* 42, 4 (2023), 1–13.

Zerong Zheng, Tao Yu, Qionghai Dai, and Yebin Liu. 2021. Deep Implicit Templates for 3D Shape Representation. In *IEEE Conference on Computer Vision and Pattern Recognition (CVPR)*. 1429–1439.

Chenyang Zhu, Renjiao Yi, Wallace Lira, Ibraheem Alhashim, Kai Xu, and Hao Zhang. 2017. Deformation-Driven Shape Correspondence via Shape Recognition. *ACM Transactions on Graphics (ToG)* 36, 4 (2017), 1–12.

Junzhe Zhu, Yuanchen Ju, Junyi Zhang, Muhan Wang, Zhecheng Yuan, Kaizhe Hu, and Huazhe Xu. 2024. DenseMatcher: Learning 3D Semantic Correspondence for Category-Level Manipulation from a Single Demo. In *International Conference on Learning Representations (ICLR)*.

Aleksei Zhuravlev, Zorah Lähner, and Vladislav Golyanik. 2025. Denoising Functional Maps: Diffusion Models for Shape Correspondence. In *IEEE Conference on Computer Vision and Pattern Recognition (CVPR)*. 1–10.

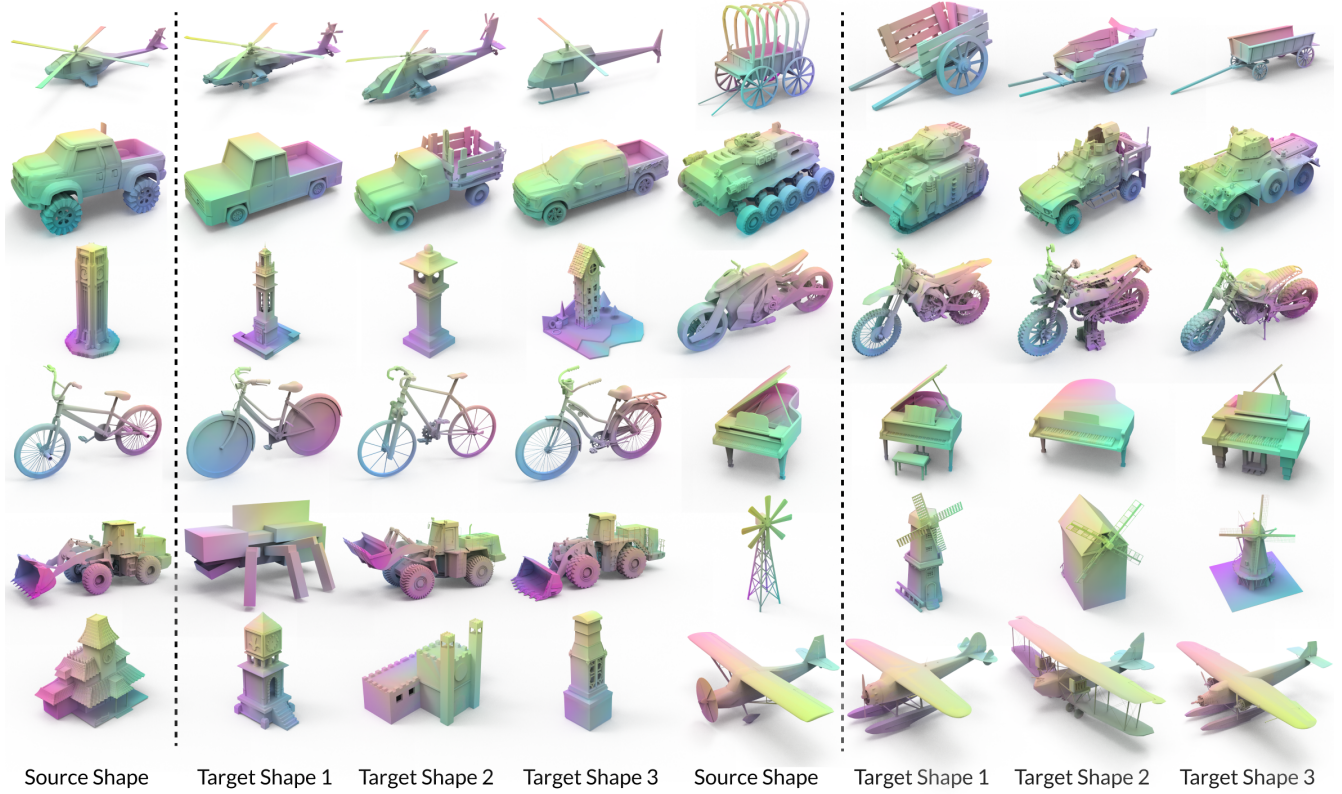


Fig. 6. Visual results for 3D semantic correspondence. Our method effectively establishes semantic correspondences between shapes with varying geometries and topologies, and generalizes well across different object categories, demonstrating robustness to structural and semantic variations.

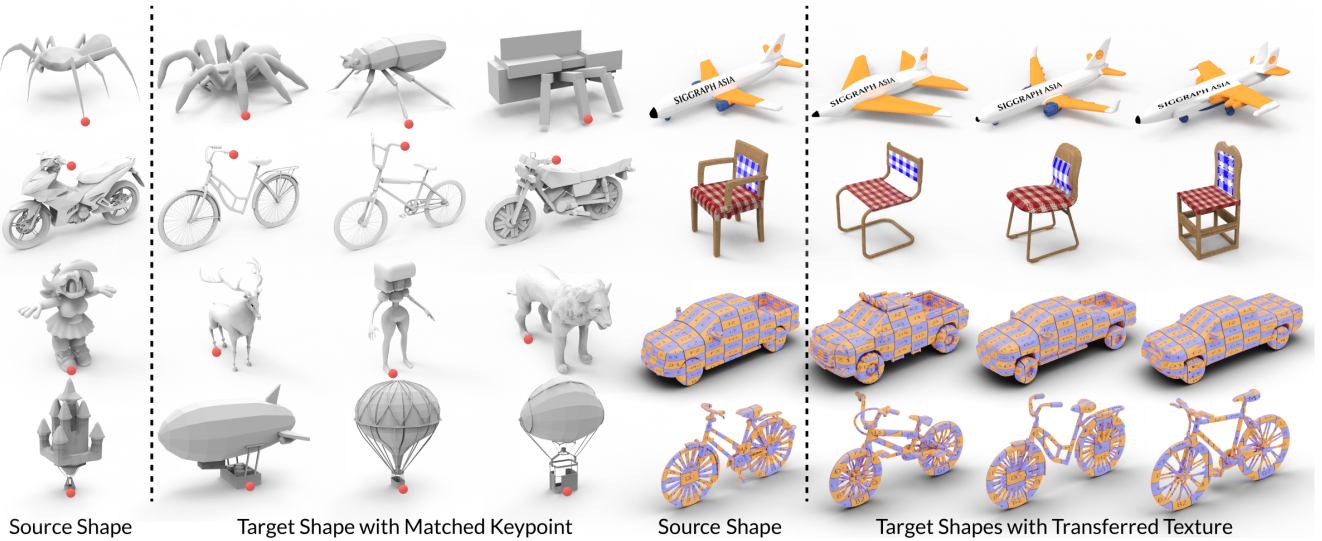


Fig. 7. Visual results for keypoint matching and texture transfer. The left part shows keypoint matching results, where our method reliably finds semantically corresponding positions across shapes, even in challenging cross-category scenarios, e.g., aligning a human foot to a deer's foot (third row). The right part demonstrates texture transfer, where detailed patterns such as airplane text are accurately preserved and mapped onto target shapes, showcasing the effectiveness of our approach. On the third and fourth rows of the right panel, we present results on transferring high-frequency chessboard textures while highlighting patch boundaries and numbering each patch. As shown, our method preserves the chessboard structure even with high-frequency patterns.

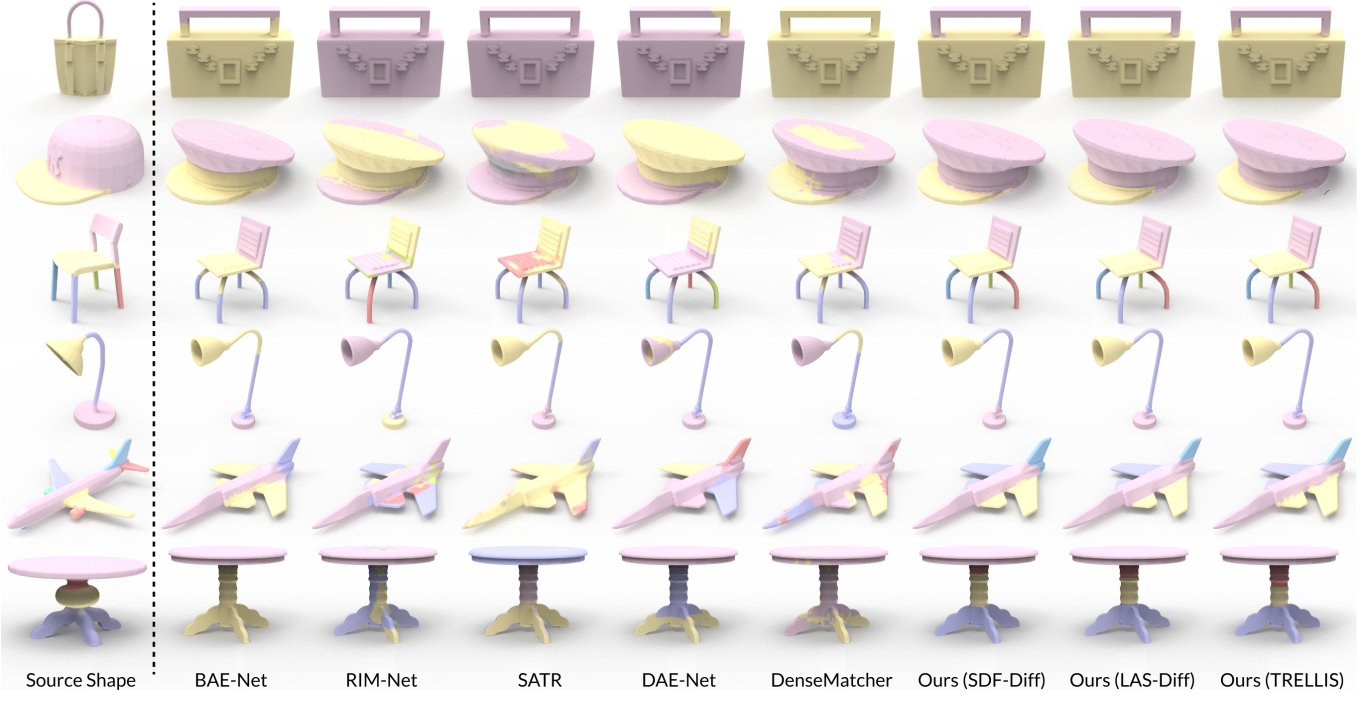


Fig. 8. Visual comparisons between our approach and other state-of-the-art methods for shape co-segmentation, including BAE-Net [Chen et al. 2019], RIM-Net [Niu et al. 2022], SATR [Abdelreheem et al. 2023b], DAE-NET [Chen et al. 2024], and DenseMatcher [Zhu et al. 2024]. We apply our approach to three different baseline architectures, i.e., SDF-Diffusion [Shim et al. 2023], LAS-Diffusion [Zheng et al. 2023], and TRELLIS [Xiang et al. 2025], all of which achieve more accurate and consistent co-segmentation results than prior methods, especially in challenging regions such as label boundaries and part connections.

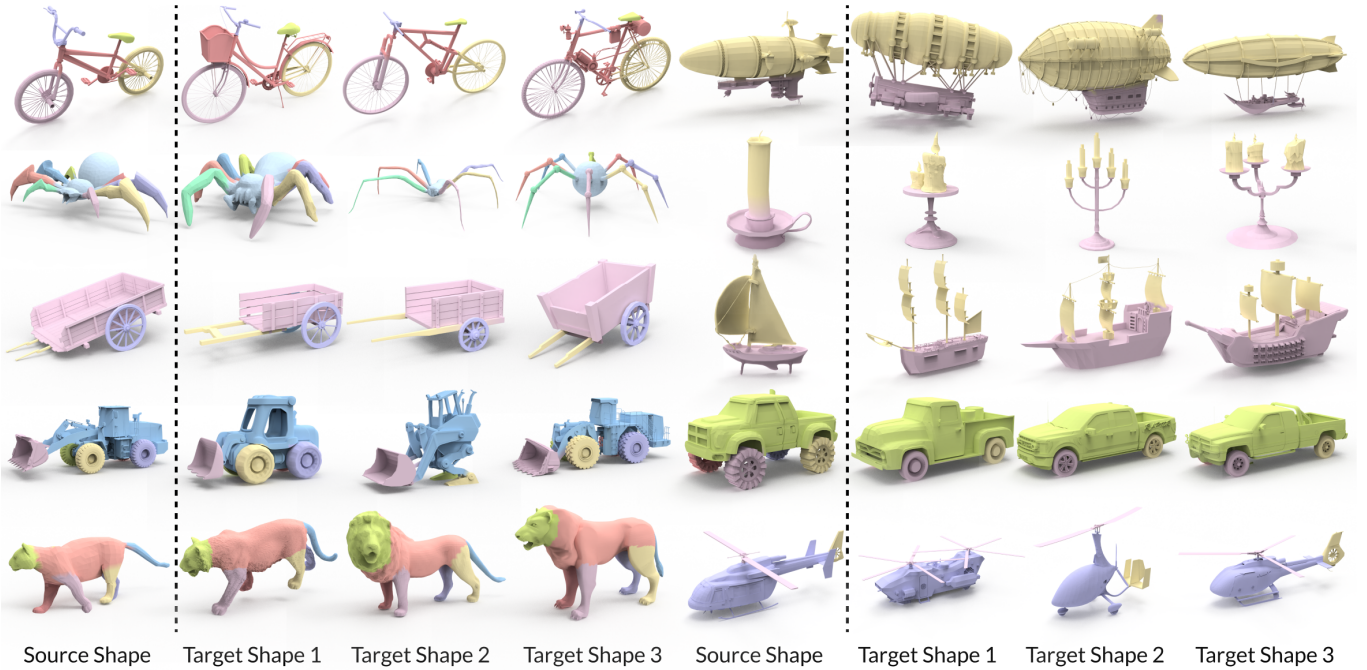


Fig. 9. Visual results for shape co-segmentation. Our method delivers precise and semantically meaningful co-segmentation beyond simple spatial alignment. As shown in the second row (right), our method accurately co-segments the candle and holder, despite large variations in their relative positions.